Available online at www.sciencedirect.com
SCIENCE DIRECT®
International Journal of Heat and Mass Transfer 48 (2005) 4985–4994
International Journal of HEAT and MASS TRANSFER
www.elsevier.com/locate/ijhmt

Effect of compressibility on gaseous flows in a micro-tube

Yutaka Asako *, Kenji Nakayama, Tetsuya Shinozuka

Department of Mechanical Engineering, Tokyo Metropolitan University, 1-1 Minami-Osawa, Hachioji, Tokyo 192-0397, Japan

Received 13 August 2004
Available online 19 August 2005

Abstract

A product of friction factor and Reynolds number ($f \cdot Re$) of gaseous flow in a quasi-fully developed region of a micro-tube was obtained numerically and experimentally. Two-dimensional compressible momentum and energy equations were solved for a wide range of Reynolds number and Mach number for both 'no heat conduction' and isothermal flow conditions. It was found from numerical results that the product of friction factor and Reynolds number ($f \cdot Re$) in a quasi-fully developed region is expressed as a function of Mach number. The tube cutting method was adopted to obtain the pressure variation along the tube. Fused silica tubes of nominal diameter of 150 μm, were used for experiments. The experimental results also indicate that ($f \cdot Re$) is a function of Mach number.

Keywords: Micro-tube; Gaseous flow; Friction factor; Compressibility

1. Introduction

Fabrication of small devices has increased the needs for understanding of fluid flow and heat transfer in micro-geometries. In case of gaseous flow, it is well known that the rarefaction (the slip on the surface), the surface roughness and the compressibility have significant effect on these results, separately or simultaneously. Since the analytical work by Prud'homme et al. [1] who performed a two-dimensional analysis for isothermal and laminar flow of an ideal gas in a straight micro-tube, many experimental and numerical investigations have been undertaken. Literatures are surveyed in a paper by Turner et al. [2].

Recently, Asako et al. [3] performed computational investigations on the effect of the compressibility for the wide range of Re and Mach number flows in parallel-plate micro-channels whose height ranges from 10 to 100 μm. They found that $f \cdot Re$ in the quasi-fully developed region where the gaseous flow is accelerated, is a function of the Mach number and obtained the correlation for $f \cdot Re$ and Mach number. They also compared their numerical results with experimental data by Turner et al. [4] and found that both results agree well. As a consequence, the flow rate for the specified inlet and outlet pressures could be predicted by using the correlation for $f \cdot Re$ and Mach number.

The value of $f \cdot Re$ in a quasi-fully developed region of a micro-tube might be a function of the Mach number. The pressure variation along a micro-tube had been experimentally obtained by Li et al. [5]. However, the values of $f \cdot Re$ calculated from their pressure data are scattered. This is the motivation of the present study

* Corresponding author. Tel.: +81 426 77 2711; fax: +81 426 77 2701.
E-mail address: asako@ecomp.metro-u.ac.jp (Y. Asako).

0017-9310/$ - see front matter © 2005 Elsevier Ltd. All rights reserved.
doi:10.1016/j.ijheatmasstransfer.2005.05.039

Nomenclature

D	diameter, m	T	temperature, K
f_d	Darcy's friction factor Eq. (12)	u, v	velocity components, m/s
f_f	modified Fanning's friction factor Eq. (13)	x, r	coordinates, m
G	mass flow rate per unit area, kg/(m^2 s)	ϕ	dissipation function Eq. (6)
h	water head, m	γ	specific heat ratio
i	specific internal energy, J/kg	μ	viscosity, Pa s
k	correction coefficient	ρ	density, kg/m^3
ℓ	channel length, m	τ	shear stress, N/m^2
$\dot{m}$	mass flow rate, kg/s		
Ma	Mach number Eq. (10)	*Subscripts*	
n	correction coefficient	ave	averaged value in a cross-section
p	pressure, Pa	in	inlet
Q	volumetric flow rate, m^3/s	out	outlet
R	gas constant, J/(kg K)	stg	stagnation value
Re	Reynolds number Eq. (10)		

to obtain $f \cdot Re$ in a quasi-fully developed region of a micro-tube.

2. Formulation

2.1. Governing equations

The problem is modeled as a micro-tube with a chamber at the stagnation temperature, T_{stg}, and the stagnation pressure, p_{stg}, attached to its upstream section as shown in Fig. 1. The flow is assumed to be steady, two-dimensional and laminar. The fluid is assumed to be an ideal gas with a specific heat ratio of $\gamma = 1.4$ and a gas constant of $R = 287$ J/(kg K). The governing equations will be similar to those documented in our previous paper [3] except for the coordinates. To avoid duplication, only a brief description is given in this article. Although the effect of the thermal condition on the product of the friction factor and Reynolds number is quite small in the case of the parallel-plate channel of our previous study, the numerical analysis will be performed for both 'no heat conduction' and isothermal flow conditions. The governing equations can be expressed as

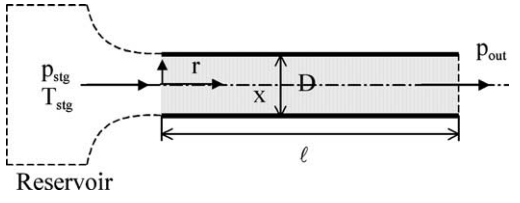

Fig. 1. A schematic diagram of problem.

$$\frac{\partial \rho u}{\partial x} + \frac{1}{r}\frac{\partial \rho r v}{\partial r} = 0 \tag{1}$$

$$\frac{\partial \rho u u}{\partial x} + \frac{1}{r}\frac{\partial \rho r u v}{\partial r} = -\frac{\partial p}{\partial x} + \frac{\partial \tau_{xx}}{\partial x} + \frac{1}{r}\frac{\partial}{\partial r}(r\tau_{rx}) \tag{2}$$

$$\frac{\partial \rho u v}{\partial x} + \frac{1}{r}\frac{\partial \rho r v v}{\partial r} = -\frac{\partial p}{\partial r} + \frac{\partial \tau_{rx}}{\partial x} + \frac{1}{r}\frac{\partial}{\partial r}(r\tau_{rr}) - \frac{\tau_{\theta\theta}}{r} \tag{3}$$

where

$$\begin{aligned}
\tau_{xx} &= \mu\left\{2\frac{\partial u}{\partial x} - \frac{2}{3}\left(\frac{\partial u}{\partial x} + \frac{1}{r}\frac{\partial r v}{\partial r}\right)\right\} \\
\tau_{xr} &= \tau_{rx} = \mu\left(\frac{\partial v}{\partial x} + \frac{\partial u}{\partial r}\right) \\
\tau_{rr} &= \mu\left\{2\frac{\partial v}{\partial r} - \frac{2}{3}\left(\frac{\partial u}{\partial x} + \frac{1}{r}\frac{\partial r v}{\partial r}\right)\right\} \\
\tau_{\theta\theta} &= \mu\left\{2\frac{v}{r} - \frac{2}{3}\left(\frac{\partial u}{\partial x} + \frac{1}{r}\frac{\partial r v}{\partial r}\right)\right\}
\end{aligned} \tag{4}$$

The energy equation for the 'no heat conduction' flow condition can be expressed as

$$\frac{\partial \rho u i}{\partial x} + \frac{1}{r}\frac{\partial \rho r v i}{\partial r} = -p\left(\frac{\partial u}{\partial x} + \frac{1}{r}\frac{\partial r v}{\partial r}\right) + \phi \tag{5}$$

where

$$\begin{aligned}
\phi = {} & 2\mu\left[\left(\frac{\partial u}{\partial x}\right)^2 + \left(\frac{v}{r}\right)^2 + \left(\frac{\partial v}{\partial r}\right)^2\right] \\
& - \frac{2\mu}{3}\left(\frac{\partial u}{\partial x} + \frac{1}{r}\frac{\partial r v}{\partial r}\right)^2 + \mu\left(\frac{\partial u}{\partial r} + \frac{\partial v}{\partial x}\right)^2
\end{aligned} \tag{6}$$

As can be seen, heat conduction terms are neglected for the case of the 'no heat conduction' flow. Since zero thermal conductivity is considered for this case, the wall heat flux becomes zero.

The isothermal flow is obtained when the gas has an infinite thermal conductivity. The energy equation for the isothermal condition can be expressed as

$$i = i_{\mathrm{in}} \tag{7}$$

where i_{in} is the specific internal energy at the inlet. That is, the tube wall temperature is the same as the fluid temperature at the inlet. Note that the energy Eq. (5) is solved when the flow is the 'no heat conduction' flow and Eq. (7) is used instead of Eq. (5) when the flow is the isothermal flow.

The equation of the state for the ideal gas is expressed by

$$i = \frac{1}{\gamma - 1}\frac{p}{\rho} \tag{8}$$

Note that the governing equations considered are identical with ones for gaseous flow in a conventional sized channel.

Furthermore, with the assumptions of no slip boundary condition, uniform inlet velocity, pressure, density and specific internal energy and specified pressure, p_{out}, at the outlet, the boundary conditions can be expressed as follows:

$$\begin{aligned}
&\text{on the walls } (r = 0.5D)\text{: } u = v = 0, \partial i/\partial r = 0\\
&\quad \text{(for 'no heat conduction' flow)}\\
&\quad i = i_{\mathrm{in}} \text{(for isothermal flow)}\\
&\text{on the symmetric axis } (r = 0)\text{: } \partial u/\partial r = 0, v = 0\\
&\text{at the inlet } (x = 0)\text{: } u = u_{\mathrm{in}}, v = 0,\ p = p_{\mathrm{in}},\ \rho = \rho_{\mathrm{in}},\ i = i_{\mathrm{in}}\\
&\text{at the outlet } (x = \ell)\text{: } p = p_{\mathrm{out}}
\end{aligned} \tag{9}$$

The velocity, the pressure and the density at the inlet of the tube are obtained by the stagnation treatment documented in a literature by Karki [6]. That is, the static pressure at the inlet is obtained by linear extrapolation from the interior of the computational domain. From this extrapolated pressure and the given stagnation values, the velocity, density and specific internal energy at the inlet are calculated with the assumption of the isentropic flow. Then, solving the governing equations, the values in the interior domain are obtained. This process is repeated until the convergence is achieved.

2.2. Reynolds and Mach numbers and friction factors

Attention will now be focused on the calculation of the Reynolds number and Mach number that will be defined as

$$Re = \frac{u_{\mathrm{ave}} D}{\mu/\rho_{\mathrm{ave}}}, \quad Ma = \frac{u_{\mathrm{ave}}}{\sqrt{\gamma(\gamma-1)i_{\mathrm{ave}}}} \tag{10}$$

where u_{ave}, ρ_{ave} and i_{ave} are the average velocity, density and specific internal energy at a cross-section as follows:

$$\begin{aligned}
u_{\mathrm{ave}} &= \frac{8}{D^2}\int_0^{D/2} ru\,\mathrm{d}r, \quad \rho_{\mathrm{ave}} = \int_0^{D/2} \rho ru\,\mathrm{d}r \Big/ \int_0^{D/2} ru\,\mathrm{d}r,\\
p_{\mathrm{ave}} &= \frac{8}{D^2}\int_0^{D/2} rp\,\mathrm{d}r, \quad i_{\mathrm{ave}} = \frac{1}{\gamma-1}\frac{p_{\mathrm{ave}}}{\rho_{\mathrm{ave}}}
\end{aligned} \tag{11}$$

Note that the Re is constant along the tube but the Ma varies along the tube.

The Darcy friction factor is defined as

$$f_{\mathrm{d}} = \frac{-2D}{\rho_{\mathrm{ave}} u_{\mathrm{ave}}^2}\left(\frac{\mathrm{d}p_{\mathrm{ave}}}{\mathrm{d}x}\right) \tag{12}$$

The modified Fanning friction factors (four times of Fanning friction factor) for the 'no heat conduction' flow and for the isothermal flow, respectively, are defined as [2]

No heat conduction flow:

$$\begin{aligned}
f_{\mathrm{f}} &= \frac{4\tau_{\mathrm{w}}}{\frac{1}{2}\rho_{\mathrm{ave}} u_{\mathrm{ave}}^2}\\
&= \frac{2D}{p_{\mathrm{ave}}}\left(\frac{\mathrm{d}p_{\mathrm{ave}}}{\mathrm{d}x}\right) - \frac{2D}{\rho_{\mathrm{ave}} u_{\mathrm{ave}}^2}\left(\frac{\mathrm{d}p_{\mathrm{ave}}}{\mathrm{d}x}\right) - \frac{2D}{T_{\mathrm{ave}}}\left(\frac{\mathrm{d}T_{\mathrm{ave}}}{\mathrm{d}x}\right)
\end{aligned} \tag{13a}$$

Isothermal flow:

$$f_{\mathrm{f}} = \frac{4\tau_{\mathrm{w}}}{\frac{1}{2}\rho_{\mathrm{ave}} u_{\mathrm{ave}}^2} = \frac{2D}{p_{\mathrm{ave}}}\left(\frac{\mathrm{d}p_{\mathrm{ave}}}{\mathrm{d}x}\right) - \frac{2D}{\rho_{\mathrm{ave}} u_{\mathrm{ave}}^2}\left(\frac{\mathrm{d}p_{\mathrm{ave}}}{\mathrm{d}x}\right) \tag{13b}$$

Eqs. (13a) and (13b) are derived from correlations for a one-dimensional compressible adiabatic and isothermal flows in a channel with a constant cross-section. The first term of the right-hand side of the equations represents the acceleration loss.

2.3. Numerical solutions

The numerical methodology is based on the Arbitrary-Lagrangian–Eulerian (ALE) method developed by Amsden et al. [7]. The detailed description of the ALE method is documented in the literature and will not be given here. The computational domain is divided into quadrilateral cells. The velocity components are defined at the vertices of the cell and other variables such as pressures, specific internal energy and density are assigned at the cell centers. The velocities on the axisymmetric line ($r = 0$) were obtained from the axisymmetric condition. The number of cells in the x-direction was 200. The cell size gradually increased in the x-direction along the tube. The number of cells in r-direction was fixed at 20 for all the computations. This grid alignment was determined from results of our previous grid dependency test [3]. The ALE method is a time marching method. The value of 10^{-4} was used for the convergence criterion of Newton–Raphson iteration.

3. Experimental setup

3.1. Measurement principle

The pressure variation along the tube was obtained by the tube cutting method proposed by Li et al. [5]. The details of the method were documented in their paper, and therefore, only a brief description will be given here. The basic principle of the tube cutting method is based on the following fact: the mass flow rate $\dot{m}$ corresponds to the outlet pressure (back pressure) p_{out} when the stagnation pressure p_{stg} and the stagnation temperature T_{stg} are fixed. That is, the characteristics of fluid flow in a micro-tube can be determined by three parameters: p_{stg}, T_{stg} and p_{out}. The thermal boundary condition of the tube wall should be identical.

The measurement principle is shown in Fig. 2, in which tube 1 and tube 2 are micro-tubes with same diameter. The pressures of both tubes at the same location from the inlet, the location M, are identical when the stagnation pressure p_{stg}, the stagnation temperature T_{stg} and the mass flow rate $\dot{m}$ of both tubes are identical. Therefore, the pressure variation along the micro-tube can be obtained indirectly by measuring the pressures at the outlet of micro-tubes with different length under the condition of identical p_{stg}, T_{stg} and $\dot{m}$. It can be considered that the pressure at the outlet of the tube and the back pressure are identical. Therefore, the back pressure was measured instead of the pressure at the outlet.

3.2. Experimental setup

A schematic diagram of the experimental setup is shown in Fig. 3. Pictures of the inlet and outlet chambers and the test micro-tube are shown in Fig. 4. Compressed nitrogen gas flows through a single stage regulator and a desiccant tube to an inlet chamber. The gas pressure was measured at the inlet chamber

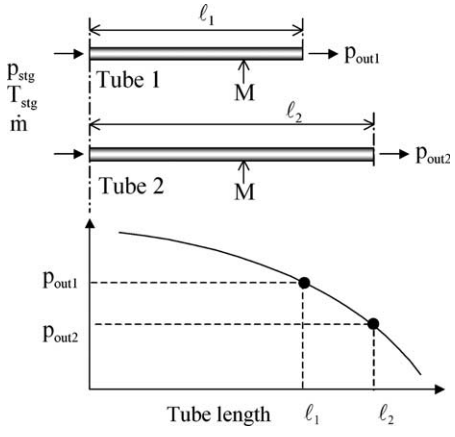

Fig. 2. Measurement principle.

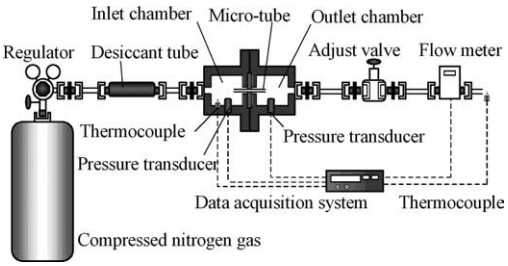

Fig. 3. A schematic diagram of experimental setup.

by a pressure transducer (Valcom, VESX500, max: 500 kPa, linearity: 0.25%). The gas temperature was also measured by a type-T thermocouple. The gas passes through a test micro-tube into an outlet chamber. The gas pressure was also measured at the outlet chamber. A flow rate regulating valve (Kofloc, 2412T) was located downstream of the outlet chamber to provide precise control of the flow rate. The flow rate was measured downstream of the pressure regulating valve by a flow meter (Kofloc, 3300, max: 4.1×10^{-6} kg/s, accuracy: $\pm 1\%$ F.S.). The exit of the flow meter was open to the atmosphere. The atmospheric pressure was measured by a mercurial barometer (Isuzu fortin barometer, minimum readings: 1/10 mm Hg). The signals from the pressure transducers and the flow meter were connected to a data acquisition system (Eto Denki, CADAC21).

3.3. Micro-tube

A fused silica tube (Upchurch scientific, FS115) was used for the test micro-tube whose nominal diameter was 150 μm. A picture of the cross-section of the silica tube and an AFM surface image of the inner surface by an atomic force microscope (Shimadzu, SPM9500) are shown in Fig. 5. The surface roughness of the inner surface in the area of 0.5×0.5 μm^2 is less than about 5 nm. The inner surface of the tube is quite smooth. The outer surface of the tube is coated by polyimide and its outer diameter is 360 μm. The length of the micro-tube was measured with a tool microscope with a moving stage (Nikon V12B, min: 1 μm).

The inner diameter of micro-tubes was obtained by flowing water in the tube. A schematic diagram of the setup is shown in Fig. 6. The mass flow rate was measured by weighting the volume of water accumulated at the outlet reservoir over the period of 600 s. An electric balance (A&D, ER-180A, min: 0.1 mg) was used for weight measurement. The measurement was conducted under the condition of $Re \approx 8.5$. The accumulated water weight ranged from 0.6 to 0.8 g. There exists evaporation from the outlet reservoir. The lost weight by evaporation during 600 s was also measured after the accumulated water measurement and the accumulated

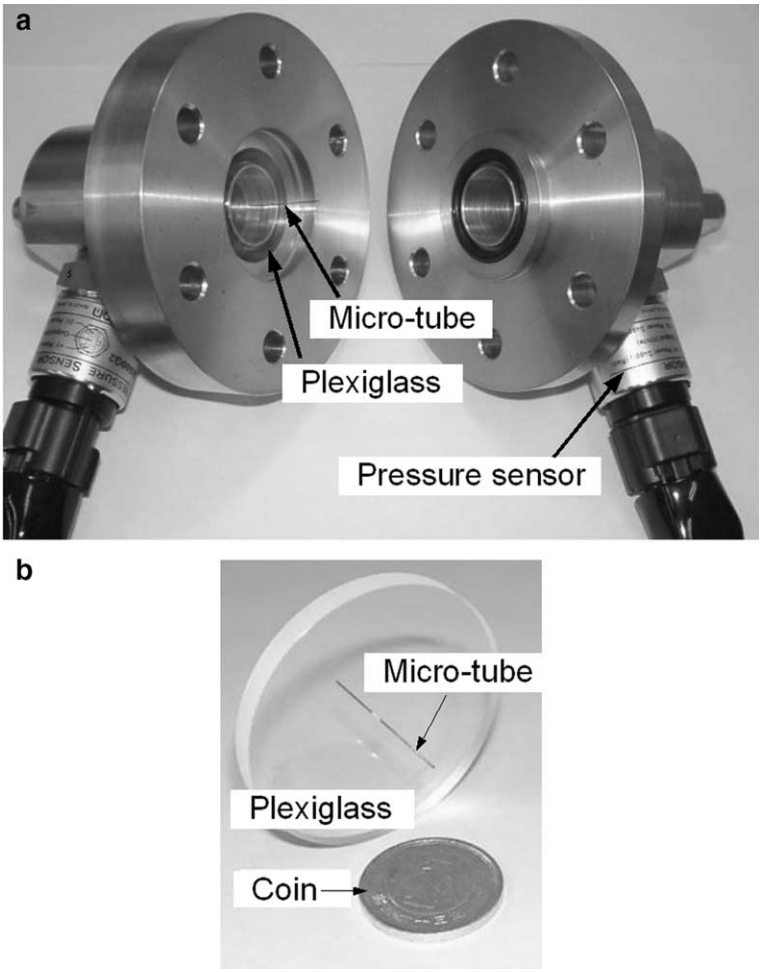

Fig. 4. Pictures of (a) inlet and outlet chambers and (b) test micro-tube.

water weight was corrected. Percentage of the lost weight to the accumulated water weight ranged from 2% to 4% depending on the weather. Substituting the volumetric flow rate $\dot{Q}$ $(= \dot{m}/\rho)$ which is calculated from the measured mass flow rate, into the following equation, the inner tube diameter was obtained.

$$\pi D^4 \rho g h - 64 \mu n D \dot{Q} = 128 \mu \ell \dot{Q} + \frac{16}{\pi} k \rho \dot{Q}^2 \tag{14}$$

Note that Eq. (14) was derived from the assumption of the Hagen–Poiseuille flow [9]. The second term in the left-hand side of the equation represents the end effect correction and the second term in the right-hand side of the equation represents the kinetic energy correction. The h is the water head. The n and k are the length correction and the kinetic energy correction coefficients, respectively, and they are $n = 0.7$ and $k = 1.12$.

The representative uncertainties are as follows: tube length ℓ, ± 1 μm, water head h, ± 0.2 mm, water temperature, ± 0.2 K, weight, ± 0.1 mg, time, ± 0.1 s. From these values, the uncertainty of the tube diameter is estimated as $\pm 0.16\%$. This corresponds to ± 0.2 μm in diameter.

Measurements were conducted for three times to an identical tube. An average of them was regarded as the inner diameter. Because of the measurement principle of the tube cutting method, a pair of tubes with an identical diameter and different lengths should be prepared. Then, the inner diameter of over 30 tubes was measured. Measured length and diameter of tubes are plotted in Fig. 7. Only three pairs of tubes (A30–A35, B35–B40 and C45–C50) can be used for the next gaseous flow experiment. A diameter and length of tubes used for the next gaseous flow experiment are tabulated in Table 1. The diameter difference of the pair of the tubes used for the next gaseous flow experiment is less than 0.1 μm. The effect of the diameter difference on the friction factor evaluation will be discussed later.

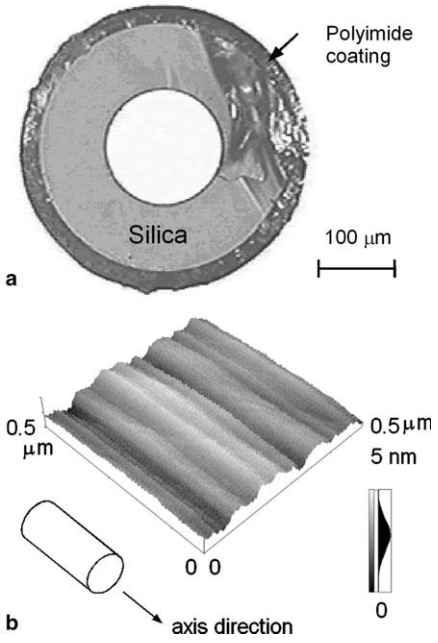

Fig. 5. Pictures of fused silica tube of (a) a cross-section and (b) AFM image of inner surface.

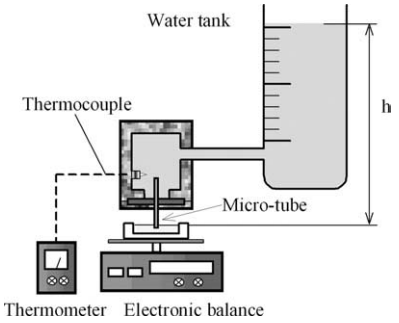

Fig. 6. Experimental setup for measurement of tube diameter.

3.4. Procedure and data reduction

The pressure regulator was adjusted to make the pressures at the inlet of the pair of the tubes identical. The pressure difference was less than 0.24%. The flow rate regulating valve was also adjusted to make the mass flow rates of the pair of the tubes identical. The difference of the mass flow rates was less than 0.25%. The temperature difference at the inlet was less than 3.7 K The effect of these inconsistencies on the friction factor evaluation will be discussed later.

The measurements were conducted after the pressure at the inlet chamber and the mass flow rate were adjusted. Data sets were collected for 10 min with interval of 5 s. All data were averaged and data reduction for the

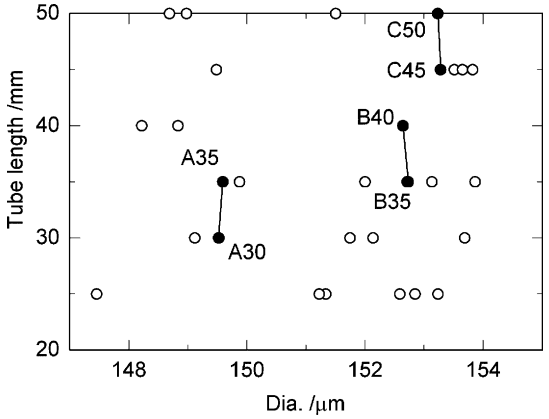

Fig. 7. Length and diameter of micro-tubes.

Darcy and Fanning friction factors was conducted. Integrating Eq. (12) from ℓ_1 to ℓ_2 with the assumption of the isothermal flow, the following equation for the Darcy friction factor is obtained.

$$f_{\mathrm{d}} = \frac{2D}{\rho, u_{\mathrm{ave}}^2}\left(\frac{p_{\mathrm{out1}} - p_{\mathrm{out2}}}{\Delta \ell}\right) \tag{15}$$

where p_{out1} and p_{out2} are the pressures at the outlet chamber of the shorter and longer tubes, respectively. Note that the Darcy friction factor includes both the viscous friction loss and the loss due to flow acceleration.

Integrating Eq. (13b) from ℓ_1 to ℓ_2 with the assumption of the isothermal flow, the following equation for the modified Fanning friction factor is obtained [8].

$$f_{\mathrm{f}} = \frac{4\tau_{\mathrm{w}}}{\frac{1}{2}\rho, u_{\mathrm{ave}}^2} = \frac{D}{\Delta \ell}\left[\frac{p_{\mathrm{out1}}^2 - p_{\mathrm{out2}}^2}{RT\dot{G}^2} - 2\ln\left(\frac{p_{\mathrm{out1}}}{p_{\mathrm{out2}}}\right)\right] \tag{16}$$

where $\dot{G}$ is the mass flow rate per unit area. The Fanning friction factor definition includes only the viscous wall friction loss and the second term in the right-hand side of Eq. (16) represents the acceleration loss.

The representative uncertainties are as follows: tube length, ℓ, ± 1 μm, pressure, p, ± 1.25 kPa, flow rate, $\pm 4 \times 10^{-8}$ kg/s, time, ± 0.1 s. Since the pressures at the outlet, p_{out1} and p_{out2}, were measured by the same pressure sensor, the uncertainty of pressure difference, $p_{\mathrm{out1}} - p_{\mathrm{out2}}$, is mainly due to the reproducibility of the pressure sensor. The reproducibility of the pressure sensor is 0.125%, therefore, the uncertainty of pressure difference, $p_{\mathrm{out1}} - p_{\mathrm{out2}}$, which ranges from 5 to 28 kPa, is ± 0.625 kPa. From these values, the uncertainty of the friction factor can be estimated as $\pm 12.5\%$.

Supplementary numerical computations were conducted to assess the effects of the inconsistencies of the inlet conditions and the tube diameter on the friction factor quantitatively. The assumed inlet conditions were the stagnation pressure $p_{\mathrm{stg}} = 300$ kPa, the stagnation temperature $T_{\mathrm{stg}} = 300$ K and the mass flow rate $\dot{m} = 4.058 \times 10^{-6}$ kg/s. It was also assumed that the

Table 1
Diameter and length of micro-tubes

	A30	A35	B35	B40	C45	C50
D/μm	149.5	149.6	152.7	152.6	153.3	153.2
ℓ/mm	30.741	34.600	32.995	40.600	45.939	50.096

Table 2
Effects of inconsistency of inlet conditions on f_d

#	D/μm	ℓ/mm	p_{stg}/kPa	T_{stg}/K	$\dot{m}$/kg s^{-1}	p_{out1}/kPa	p_{out2}/kPa	f_d	Error/%
1	150	*40*	300	300	4.058×10^{-6}	–	170.84	–	–
2	150	35	300	300	4.058×10^{-6}	190.09	–	0.04436	–
3	*151*	35	300	300	4.058×10^{-6}	194.71	–	0.05501	24.0
4	*150.1*	35	300	300	4.058×10^{-6}	190.57	–	0.04546	2.49
5	150	35	300	300	*4.068* $\times10^{-6}$	189.49	–	0.04351	−1.92
6	150	35	*299.28*	300	4.058×10^{-6}	188.77	–	0.04127	−6.91
7	150	35	300	*296*	4.058×10^{-6}	192.47	–	0.04984	12.4

lengths of the shorter and longer tubes were 35 and 40 mm and the tube diameter was 150 μm. The inlet conditions and the tube diameter for the assessment and results are tabulated in Table 2. Computations for the cases 1 and 2 were conducted to obtain the friction factor for the assumed condition. The computation for the case 3 was conducted to assess the inconsistency of the shorter tube diameter. That is, the friction factor for the situation where the shorter tube with the diameter of 151 μm is used instead of 150 μm, was obtained from p_{out1} of case 3 and p_{out2} of case 1. The case 4 was also conducted to assess the inconsistency of the shorter tube diameter (150.1 μm). The cases 5, 6 and 7 were conducted to assess the inconsistencies of the mass flow rate (0.25% higher case), the stagnation pressure (0.24% lower case) and the stagnation temperature (4 K lower case), respectively.

As a consequence, it is found that 24% higher friction factor is obtained by the tube cutting method when the shorter tube whose diameter is 151 μm, is used instead of 150 μm. The similar result is obtained when the friction factor of the Poiseuille flow is obtained by the tube cutting method. The pressure drop between the inlet and outlet of the Poiseuille flow is proportional to $1/D^4$. This is the reason why the tube cutting method is so sensitive to the tube diameter. It is also found that the effects of the inconsistency of the stagnation temperature on the friction factor are relatively high.

4. Results and discussions

4.1. Numerical results

The computations were performed for five micro-tubes. The tube diameter and length are tabulated in Table 3. The outlet pressure and the stagnation temperature were fixed at $p_{out} = 100$ kPa and 300 K. The stagnation pressure was varied. That is, computations were performed for each tube changing the stagnation pressure. The stagnation pressure, p_{stg} is also listed in Table 3.

The contour plots of the pressure and temperature for the flow in a tube of $D = 20$ μm and $\ell = 4$ mm are presented in Fig. 8(a) and (b), respectively, and the velocity vector is presented in Fig. 8(c). The reference arrow in the figure represents a velocity of 100 m/s. The results are for the 'no heat conduction' flow condition and for the stagnation pressure, $p_{stg} = 300$ kPa. The pressure at any cross-section of the tube is almost uniform, and it decreases along the tube. The pressure variation along the tube is plotted in Fig. 9. The pressure gradient becomes steep near the outlet. Fig. 8(b) represents the temperature contours in the tube. The temperature in the core region of the tube decreases as a result of acceleration. On the other hand, the temperature rise can be seen near the walls due to viscous heat dissipation. The similar tendency can be seen in a case of parallel-plate channel [3]. Fig. 8(c) represents the velocity vector in the tube. The flow in the tube is accelerated and the average velocity increases. This is due to the

Table 3
Tube dimensions and stagnation pressure for numerical analysis

Tube	D/μm	ℓ/mm	p_{stg}/kPa
#1	10	2	300, 400
#2	20	4	300, 400
#3	50	10	300, 400
#4	100	20	200, 300
#5	130	40	250

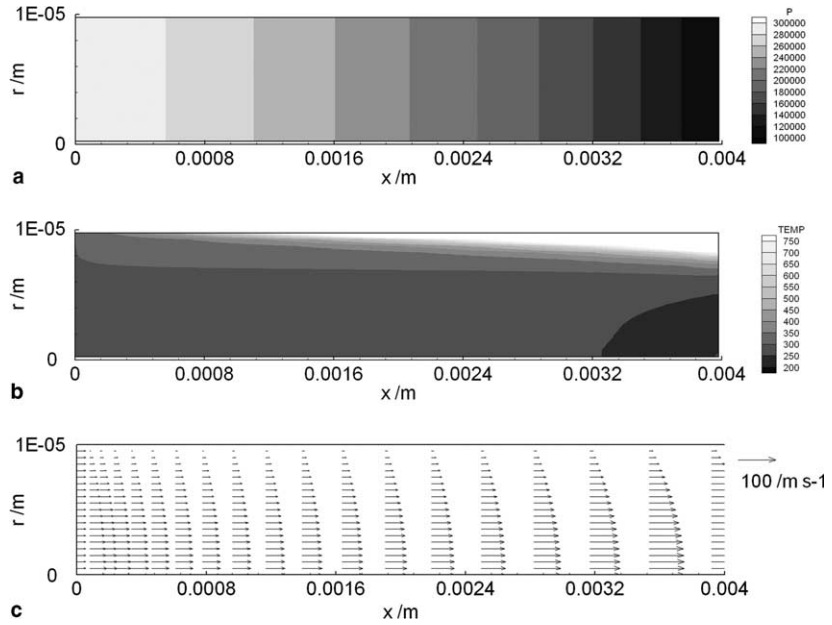

Fig. 8. Contour plots of (a) pressure, (b) temperature and (c) velocity vector (no heat conduction flow: $D = 20$ μm, $\ell = 0.004$ m and $p_{stg} = 300$ kPa).

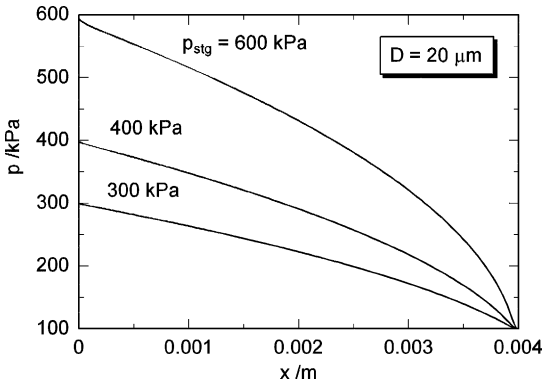

Fig. 9. Pressure variation along tube (no heat conduction flow: $D = 20$ μm, $\ell = 0.004$ m).

volume expansion of the gas caused by the pressure drop. However, the velocity profile is nearly parabolic.

The values of $f_f \cdot Re$ and $f_d \cdot Re$ for 'no heat conduction' and isothermal conditions are plotted as a function of Mach number in Fig. 10(a) and (b), respectively. The solid line in the figure represents the correlation for the $f \cdot Re$ and Mach number that is obtained by a polygonal curve fit as:

$$f_f \cdot Re = 64 + 2.703 \times Ma + 93.89 \times Ma^2 \quad (17)$$

$$f_d \cdot Re = 64 - 11.99 \times Ma + 263.7 \times Ma^2 \quad (18)$$

The dashed lines in Fig. 10(a) represent the range of ±5% of Eq. (17). As seen in the figure, all of $f_f \cdot Re$ are within the range of ±5%, The same tendency can be seen for the case of $f_d \cdot Re$.

4.2. Experimental results

The experiments were performed with three pairs of micro-tubes. The stagnation temperature was nearly 293 K. The typical stagnation pressure p_{stg}, the pressure at the outlet of longer tube, p_{out2}, are listed in Table 4. The mass flow rate $\dot{m}$, Re number and Ma number at the outlet are also listed in Table 4.

The $f_f \cdot Re$ and $f_d \cdot Re$ obtained by the experiments are plotted as a function of Mach number in Fig. 11(a) and (b), respectively. The dash–dot line in the figures represents the polygonal curve fit for the experimental data. The data obtained by the experiments are slightly scattered and however, the tendency that the $f \cdot Re$ increases with increasing the Mach number, can be seen. The solid line represents the numerically obtained correlations for $f \cdot Re$ and Mach number given by Eqs. (17) and (18). The data obtained by the experiments coincide with the numerically obtained correlations within 15%.

4.3. Prediction of pressure variation and flow rate

It is convenient if the pressure variation and flow rate can be predicted for specified inlet and outlet pressures. This could be done if the flow is assumed to be a quasi-fully developed flow in the entire region of the tube.

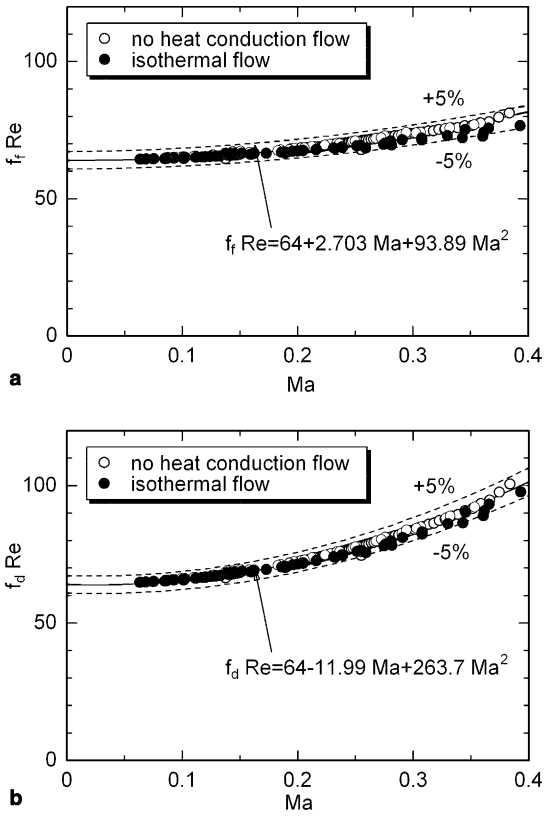

Fig. 10. Numerically obtained correlation for $f \cdot Re$. (a) $f_f \cdot Re$ and (b) $f_d \cdot Re$.

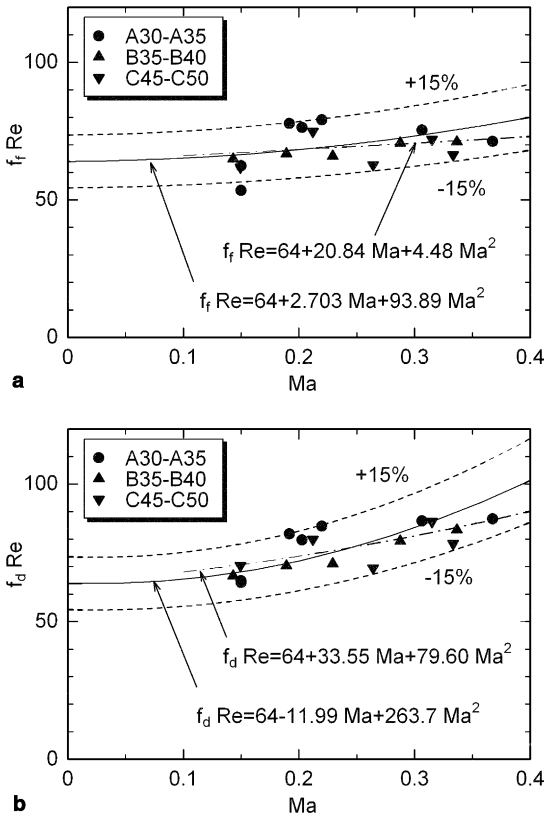

Fig. 11. Experimental results of (a) $f_f \cdot Re$ and (b) $f_d \cdot Re$.

Table 4
Typical stagnation conditions and outlet Ma number for A30–A35

#	p_{stg}/kPa	p_{out2}/kPa	$\dot{m}$/kg s^{-1}	Re	Ma_{out}
1	200	86	4.17×10^{-6}	2020	0.31
2	200	65	4.48×10^{-6}	2169	0.37
3	250	194	3.13×10^{-6}	1508	0.15
4	250	164	4.14×10^{-6}	2008	0.22
5	300	216	4.56×10^{-6}	2188	0.20

Substituting Eq. (12) into Eq. (18) with the ideal gas law, the mass conservation, $\rho_{ave}u_{ave} = \rho_{in}u_{in}$, and the assumption of isothermal flow, the following ordinary differential equation for the pressure p_{ave} and a correlation for the Ma and p_{ave} can be obtained.

$$\frac{dp_{ave}}{dx} = \frac{-\mu\sqrt{\gamma RT_{in}}Ma_{in}p_{in}}{2D^2}\left\{64 - 11.99 \times Ma_{in}\frac{p_{in}}{p_{ave}} + 263.7 \times \left(Ma_{in}\frac{p_{in}}{p_{ave}}\right)^2\right\} \quad (19)$$

$$Ma = Ma_{in}\frac{p_{in}}{p_{ave}} \quad (20)$$

If the pressure and Mach number at the inlet are given, Eq. (19) can be solved. However, in a case where the inlet and outlet pressures are specified, the inlet Mach number is unknown. In such a case, the pressure variation and the flow rate can be obtained by solving Eq. (19) iteratively with assuming the inlet Mach number.

5. Concluding remarks

The experiments for gaseous flow in micro-tubes were conducted by the tube cutting method. Two-dimensional compressible momentum and energy equations are numerically solved for a micro-tube. The following conclusions are reached.

(1) Both $f_f \cdot Re$ and $f_d \cdot Re$ are function of the Mach number and they differ from the incompressible value of 64 for a circular tube. The following correlations are obtained from the numerical results for $Ma < 0.4$.

$$f_f \cdot Re = 64 + 2.703 \times Ma + 93.89 \times Ma^2$$

$$f_d \cdot Re = 64 - 11.99 \times Ma + 263.7 \times Ma^2$$

(2) The $f \cdot Re$ obtained by experiments is slightly scattered. However, the tendency that the $f \cdot Re$ increases with increasing Mach number, can be seen.

Acknowledgement

Financial support from the Japan Society for the Promotion of Science (Grant-in-aid for Scientific Research (C) #14550192) is greatly acknowledged.

References

[1] R.K. Prud'homme, T.W. Chapman, J.R. Bowen, Laminar compressible flow in a tube, Appl. Sci. Res. 43 (1986) 67–74.

[2] S.E. Turner, H. Sun, M. Faghri, O.J. Gregory, Effect of surface roughness on gaseous flow through micro channels, 2000 IMECE, HTD-vol. 366 (2) (2000) 291–298.

[3] Y. Asako, T. Pi, S.E. Turner, M. Faghri, Effect of compressibility of gaseous flow in micro-channels, Int. J. Heat Mass Transfer 46 (16) (2003) 3041–3050.

[4] S.E. Turner, M. Faghri, O.J. Gregory, Compressible gas flow through smooth and rough microchannels, 2001 IMECE, HTD-24145 (2001) 1–4.

[5] Z. Li, D. Du, Z. Guo, The characteristics of frictional resistance for gas flow in microtubes, in: Proceedings of Symposium on Energy Engineering in the 21th Century, vol. 2, 2000, pp. 658–664.

[6] K.C. Karki, A calculation procedure for viscous flows at all speeds in complex geometries, Ph.D. thesis, University of Minnesota, 1986.

[7] A.A. Amsden, H.M. Ruppel, C.W. Hirt, SALE a simplified ALE computer program for fluid flow at all speeds, Los Alamos Scientific Lab. Report, LA-8095, 1980.

[8] F. Choquette, M. Faghri, E.J. Kenyon, B. Sunden, Compressible fluid flow in micron sized channels, ASME National Heat Transfer Conference, HTD-vol. 327, 1996, pp. 25–32.

[9] F.R. Eirich, Rheology, vol. 3, Academic Press, New York, 1960, p. 25.